Low Temperature Physics/Fizika Nizkikh Temperatur, 2016, v. 42, No. 5, pp. 455–462

Rayleigh and Wood anomalies in the diffraction of acoustic waves from the periodically corrugated surface of an elastic medium

A.A. Maradudin

Department of Physics and Astronomy, University of California, Irvine CA 92697, U.S.A.
E-mail: aamaradu@uci.edu

I. Simonsen

Department of Physics, NTNU Norwegian University of Science and Technology, NO-7491 Trondheim, Norway
Department of Petroleum Engineering, University of Stavanger, NO-4036 Stavanger, Norway

Received November 20, 2015, published online March 23, 2016

By the use of the Rayleigh method we have calculated the angular dependence of the reflectivity and the efficiencies of several other diffracted orders when the periodically corrugated surface of an isotropic elastic medium is illuminated by a volume acoustic wave of shear horizontal polarization. These dependencies display the signatures of Rayleigh and Wood anomalies, usually associated with the diffraction of light from a metallic grating. The Rayleigh anomalies occur at angles of incidence at which a diffracted order appears or disappears; the Wood anomalies here are caused by the excitation of the shear horizontal surface acoustic waves supported by the periodically corrugated surface of an isotropic elastic medium. The dispersion curves of these waves in both the nonradiative and radiative regions of the frequency-wavenumber plane are calculated, and used in predicting the angles of incidence at which the Wood anomalies are expected to occur.

PACS: **62.30.+d** Mechanical and elastic waves; vibrations;
46.40.Cd Mechanical wave propagation (including diffraction, scattering, and dispersion);
68.35.Iv Acoustical properties.

Keywords: elastic medium, surface waves, Rayleigh and Wood anomalies.

1. Introduction

It has been known for some time that while a planar, stress-free surface of a semi-infinite isotropic elastic medium does not support a surface acoustic wave of shear horizontal polarization, a periodically corrugated surface of such a medium does support a surface wave of this polarization [1–3]. It has also been known for some time that while the planar surface of a semi-infinite perfect conductor does not support a surface electromagnetic wave, a periodically corrugated surface of a perfect conductor supports a *p*-polarized surface electromagnetic wave [4,5].

There is an isomorphism between these two wave problems. The isotropic elastic medium in the former problem is the analogue of the vacuum in the latter problem, while the vacuum in the former problem is the analogue of the perfect conductor in the latter problem. The equation of motion of the single nonzero component of the displacement field of an acoustic wave of shear horizontal polarization, and the stress-free boundary condition it satisfies on the corrugated surface of the elastic medium, are the same as the Maxwell equation for the single nonzero component of the magnetic field in the vacuum, and the boundary condition on the corrugated surface of the perfect conductor. One needs only to replace the speed of bulk transverse waves c_t in the former set of equations by the speed of light in vacuums c, to obtain the latter set of equations [4].

There is, however, a significant difference between these two systems. A perfect conductor is a hypothetical medium that can be regarded as a metal in the limit as the real part of its dielectric function approaches $-\infty$. In practice such a medium is well approximated by a metal in the terahertz and microwave frequency ranges, but it is still an idealization of a real metal. In contrast, an elastic medium is a real entity, not some hypothetical limit of a real medium. Consequently, some interactions of electromagnetic

waves with a corrugated perfectly conducting surface can be studied rigorously experimentally by studying the interaction of bulk elastic waves with the stress-free corrugated surface of an elastic medium.

We note here that although we have referred to isotropic elastic media only until now, the discussion in this paper applies equally well to an elastic medium of cubic symmetry whose cube axes coincide with the coordinate axes. The speed of bulk transverse waves in this case is $c_t = (c_{44}/\rho)^{1/2}$, where c_{44} is a shear elastic modulus of the medium, and ρ is its mass density [6]. However, in what follows we will confine our attention to isotropic elastic media.

It is the fact that the interaction of an acoustic wave with the corrugated surface of an isotropic elastic medium can mimic the interaction of an electromagnetic wave with the corrugated surface of a perfect conductor that prompts this paper. In a recent paper by the present authors and their colleagues [7] the diffraction of a *p*-polarized electromagnetic wave from a perfectly conducting lamellar grating was studied by a rigorous numerical approach. That work was motivated by the desire to demonstrate that the dependence of the reflectivity and other diffraction efficiencies on the angle of incidence displays Rayleigh and Wood anomalies. These anomalies were first observed in 1902 by R.W. Wood in measurements of the angular and wavelength dependencies of the reflectivities of light diffracted from various metallic gratings [8,9]. These anomalies occurred when the magnetic vector of the incident light was parallel to the grooves of the grating (*p* polarization) and were of two types.

The first type of anomaly was a discontinuous change in the reflectivity at well-defined wavelengths for a fixed angle of incidence. These wavelengths were independent of the metal on which the grating was ruled, and were determined by the period of the grating. It was shown by Lord Rayleigh [10,11] that these anomalies occur at the wavelengths at which a diffracted order appears or disappears. For the *n*th diffracted order this occurs at the wavelengths given by $\lambda_n = a(\pm 1 - \sin\theta_0)/n$, where a is the period of the grating, θ_0 is the angle of incidence, and n is an integer. These anomalies are now called Rayleigh anomalies.

The second type of anomaly was diffuse, and extended in a wide range of wavelengths toward longer wavelengths from a Rayleigh anomaly. These anomalies generally consisted of a maximum or minimum of the intensity, and occurred only in *p* polarization when the plane of incidence was perpendicular to the grooves of the grating. The wavelength at which they occurred changed when the metal on which the grating was fabricated was changed. The explanation for these anomalies was provided by Fano [12], who showed that they are due to the excitation of the surface electromagnetic waves — surface plasmon polaritons — supported by a periodically corrugated vacuum–metal interface. The wavenumber of the surface plasmon polariton of frequency ω, $k_{spp}(\omega)$, is slightly larger than ω/c in the frequency range where the dielectric function of the metal (assumed to be real) is negative. The component of the wave vector of the incident light parallel to the surface, $k = (\omega/c)\sin\theta_0$, is smaller than ω/c. For momentum to be conserved in the interaction of the incident wave with the surface plasmon polariton the difference between these two wavenumbers must be made up. In the present case this is done by a wavenumber of the grating, $2\pi n/a$, where n is an integer. Thus, the condition for the excitation of the surface plasmon polariton is $k = k_{spp}(\omega) + 2\pi n/a$ [13].

The results of Ref. 7 showed that the diffraction of light from a periodically corrugated surface, that in the absence of the corrugations does not support surface electromagnetic waves, displays Rayleigh and Wood anomalies in the dependence of the scattering efficiencies on the angle of incidence. The mechanism responsible for the latter anomalies was the excitation by the incident field of the surface electromagnetic waves induced by the corrugations of the surface.

In light of these results it seemed of some interest to study the diffraction of waves from the periodically corrugated surface of a different medium that also supports surface waves only because of its corrugations, but unlike the surface of a perfect conductor can be accessed experimentally without difficulty. The diffraction of volume acoustic waves from the periodically corrugated surface of an isotropic elastic medium, when the plane of incidence is perpendicular to the grooves of the grating, is such a system.

Thus, in this paper, on the basis of the Rayleigh hypothesis [14], we study the diffraction of a volume acoustic wave of shear horizontal polarization from a sinusoidally corrugated surface of an isotropic elastic medium. The dependence of the reflectivity and other diffraction efficiencies on the angle of incidence is determined, as well as the dispersion curve of the surface wave of shear horizontal polarization supported by the corrugated surface in both the nonradiative and radiative regions of the frequency-wavenumber plane. These dispersion curves are used to confirm features (maxima and minima) in the angular dependencies of the efficiencies as Wood anomalies. Rayleigh anomalies are found at angles of incidence defined by the wavelength of the incident wave and the period of the grating. All of these anomalies should be observable experimentally.

2. The diffraction problem

The physical system we study consists of an isotropic elastic medium in the region $x_3 > \zeta(x_1)$, and vacuum in the region $x_3 < \zeta(x_1)$ (Fig. 1). The surface profile function $\zeta(x_1)$ is assumed to be a differentiable single-valued function of x_1 that is periodic with a period a, $\zeta(x_1 + a) = \zeta(x_1)$. The surface $x_3 = \zeta(x_1)$ is illuminated from within the elastic medium by a volume acoustic wave of shear horizontal

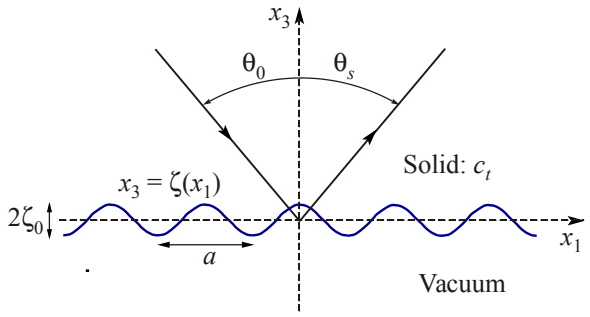

Fig. 1. A definition of the grating considered in this work, the parameters that define it, and the geometry of the diffraction of shear horizontal acoustic waves from it.

polarization of frequency ω, whose plane of incidence is the x_1x_3 plane. In this geometry the diffracted beams have the same, shear horizontal, polarization, and the plane of scattering is also the x_1x_3 plane.

The elastic displacement field in the region $x_3 > \zeta(x_1)$ thus has the form

$$\mathbf{u}(\mathbf{x};t) = (0, u_2(x_1, x_3 \mid \omega), 0)\exp(-i\omega t). \quad (1)$$

The displacement component $u_2(x_1, x_2 \mid \omega)$ satisfies the Helmholtz equation

$$\left(\frac{\partial^2}{\partial x_1^2} + \frac{\partial^2}{\partial x_3^2} + \frac{\omega^2}{c_t^2}\right) u_2(x_1, x_3 \mid \omega) = 0, \quad x_3 > \zeta(x_1), \quad (2)$$

where c_t is the speed of shear acoustic waves in the medium. The solution of Eq. (2) that satisfies the boundary conditions at infinity of an incoming incident wave and outgoing diffracted waves, and also satisfies the Bloch condition $u_2(x_1 + a, x_3 \mid \omega) = u_2(x_1, x_3 \mid \omega)\exp(ika)$, where $k = (\omega / c_t)\sin\theta_0$, with θ_0 the angle of incidence measured counterclockwise from the x_3 axis, required by the periodicity of the surface, can be written

$$u_2(x_1, x_3 \mid \omega) = \exp\left[ikx_1 - i\alpha(k,\omega)x_3\right] + \\ + \sum_{n=-\infty}^{\infty} A_n(k,\omega)\exp\left[ik_n x_1 + i\alpha(k_n,\omega)x_3\right]. \quad (3)$$

Here $k_n = k + 2\pi n / a$, and

$$\alpha(k,\omega) = \left[\left(\frac{\omega}{c_t}\right)^2 - k^2\right]^{1/2}. \quad (4)$$

The manner in which the branch cut defining the square root in Eq. (4) is determined will be described below.

The stress-free boundary condition satisfied by $u_2(x_1, x_3 \mid \omega)$ on the surface $x_3 = \zeta(x_1)$ is

$$\left\{\left[-\zeta'(x_1)\frac{\partial}{\partial x_1} + \frac{\partial}{\partial x_3}\right] u_2(x_1, x_3 \mid \omega)\right\}\Big|_{x_3=\zeta(x_1)} = 0, \quad (5)$$

that is, the normal derivative of $u_2(x_1, x_3 \mid \omega)$ is required to vanish at the surface. When we substitute Eq. (3) into Eq. (5), we obtain the equation satisfied by the amplitudes $\{A_n(k,\omega)\}$:

$$-i\left[\zeta'(x_1)k + \alpha(k,\omega)\right]\exp\left[ikx_1 - i\alpha(k,\omega)\zeta(x_1)\right] - \\ -i\sum_{n=-\infty}^{\infty} A_n(k,\omega)\left[\zeta'(x_1)k_n - \alpha(k_n,\omega)\right]\times \\ \times\exp\left[ik_n x_1 + i\alpha(k_n,\omega)\zeta(x_1)\right] = 0. \quad (6)$$

The validity of using the expansion given by the second term on the right hand side of Eq. (3) for the diffracted field, which strictly speaking is valid only outside the selvedge region, in satisfying the boundary condition (5) constitutes the Rayleigh hypothesis [14].

To solve this equation we introduce the representation

$$\exp\left[i\gamma\zeta(x_1)\right] = \sum_{p=-\infty}^{\infty} \mathcal{I}_p(\gamma)\exp\left[i\frac{2\pi p}{a}x_1\right], \quad (7)$$

so that

$$\mathcal{I}_p(\gamma) = \frac{1}{a}\int_{-a/2}^{a/2} dx_1 \exp\left[-i\frac{2\pi p}{a}x_1 + i\gamma\zeta(x_1))\right]. \quad (8)$$

By differentiating Eq. (7) with respect to x_1 we obtain a second useful result:

$$\zeta'(x_1)\exp\left[i\gamma\zeta(x_1)\right] = \sum_{p=-\infty}^{\infty} \frac{2\pi p}{a}\frac{\mathcal{I}_p(\gamma)}{\gamma}\exp\left[i\frac{2\pi p}{a}x_1\right]. \quad (9)$$

When Eqs. (7) and (9) are used in Eq. (6), the equation for the $\{A_j(k,\omega)\}$ becomes

$$\sum_{n=-\infty}^{\infty} \frac{\mathcal{I}_{m-n}(\alpha(k_n,\omega))}{\alpha(k_n,\omega)}\left[k_m k_n - \left(\frac{\omega}{c_t}\right)^2\right] A_n(k,\omega) = \\ = \frac{\mathcal{I}_m(-\alpha(k,\omega))}{\alpha(k,\omega)}\left[kk_m - \left(\frac{\omega}{c_t}\right)^2\right], \quad m = 0, \pm1, \pm2, \ldots \quad (10)$$

The diffraction efficiency of the mth diffracted beam is given by

$$e_m(k,\omega) = \frac{\alpha(k_m,\omega)}{\alpha(k,\omega)}\left|A_m(k,\omega)\right|^2. \quad (11)$$

As there is no absorption in the system we are studying, the conservation of energy in the diffraction process is expressed by

$$\sum_m{}' e_m(k,\omega) = \sum_m{}' \frac{\alpha(k_m,\omega)}{\alpha(k,\omega)} \mid A_m(k,\omega)\mid^2 = 1, \quad (12)$$

where the prime on the sum denotes that it extends over only the open channels, i.e., the ones for which $\alpha(k_m,\omega)$ is real. Finally, the reflectivity is given by

$$R(k,\omega) = e_0(k,\omega) = \left|A_0(k,\omega)\right|^2. \quad (13)$$

3. The dispersion relation for surface acoustic waves

To obtain the dispersion relation for the surface acoustic waves of shear horizontal polarization supported by the periodically corrugated surface of an isotropic elastic medium, we have only to remove the incident field from the right-hand side of Eq. (3). This is equivalent to deleting the inhomogeneous term from Eq. (10). In this way we obtain the homogeneous system of equations for the amplitudes $\{A_n(k,\omega)\}$ [3]

$$\sum_{n=-\infty}^{\infty} M_{mn}(k,\omega)A_n(k,\omega)=0, \quad m=0,\pm1,\pm2,\ldots, \quad (14)$$

where the matrix element $M_{mn}(k,\omega)$ is defined by

$$M_{mn}(k,\omega)=\frac{\mathcal{I}_{m-n}\left(\alpha(k_n,\omega)\right)}{\alpha(k_n,\omega)}\left[k_m k_n-\left(\frac{\omega}{c_t}\right)^2\right]. \quad (15)$$

The solvability condition for this system of equations, namely the vanishing of the determinant of the matrix $\mathbf{M}(k,\omega)$,

$$D(k,\omega)=\det\left[M_{mn}(k,\omega)\right]=0, \quad (16)$$

is the dispersion relation we seek.

The displacement field of the surface wave is then given by the second term on the right-hand side of Eq. (3),

$$u_2(x_1,x_3\,|\,\omega)=\sum_{n=-\infty}^{\infty} A_n(k,\omega)\exp\left[ik_n x_1+i\alpha(k_n,\omega)x_3\right]. \quad (17)$$

The solutions $\omega(k)$ of Eq. (16) are even functions of k, $\omega(-k)=\omega(k)$. They are also periodic functions of k with period $2\pi/a$, $\omega(k+2\pi/a)=\omega(k)$. Therefore, all of the solutions of Eq. (16) can be obtained if we restrict the wavenumber k to the interval $0\le k\le\pi/a$. This is called the reduced zone scheme, and we adopt it here. The resulting dispersion curve consists of an infinite number of branches of increasing frequency, of which we have determined only the three with the lowest frequencies.

In the absence of the periodic corrugations of the elastic medium the resulting planar surface does not support a true surface acoustic wave of shear horizontal polarization, only a surface skimming bulk wave whose dispersion relation is $\omega=c_t k$. In the reduced zone scheme the portions of this curve in the second, third, …, one-dimensional Brillouin zones are folded into the first Brillouin zone $-\pi/a<k\le\pi/a$, by translations to the left and to the right by suitable multiples of $2\pi/a$. The result is a zig-zag dispersion curve with a second, third, … branch in addition to the lowest frequency branch. This is called the empty lattice dispersion curve.

In the nonradiative region of the (k,ω) plane, which is defined by $|k|>\omega/c_t$, the $\{\alpha(k_n,\omega)\}$ are purely imaginary, with a positive imaginary part, for all n. From Eq. (17) we see that this result corresponds to a surface wave whose amplitude decays exponentially into the medium with increasing x_3. The solutions $\omega(k)$ of Eq. (16) in this region are real and correspond to true surface waves.

For k and ω outside the nonradiative region, i.e., inside the radiative region, some of the $\alpha(k_n,\omega)$ become complex with a positive real part, and thus produce components in the sum (17) that radiate into the elastic medium. As the resulting wave radiates into the medium it must decrease in amplitude. To describe this conversion of surface waves into bulk acoustic waves in the medium we will consider ω to be complex and k to be real. The imaginary part of ω gives the inverse lifetime of the amplitude of the leaky surface wave.

To obtain solutions of Eq. (16) that possess these properties, the branch cut that defines the square root in the definition of $\alpha(k_n,\omega)$, Eq. (4), must be chosen properly. We begin by writing

$$\omega(k)=\omega_R(k)-i\omega_I(k), \quad (18)$$

where $\omega_R(k)$ and $\omega_I(k)$ both are real, positive functions of k. A negative imaginary part of $\omega(k)$ is needed in order to have a wave whose amplitude decays in time as it propagates, due to its leakage. With Eqs. (4) and (18) we have

$$\alpha^2(k_n,\omega)=\left[\frac{\omega_R^2-\omega_I^2}{c_t^2}-k_n^2\right]-i\frac{2\omega_R\omega_I}{c_t^2}. \quad (19)$$

It has been shown [7] that if the branch cut is taken along the negative imaginary axis, $\alpha(k_n,\omega)$ has the desired properties in both the nonradiative and radiative regions of the (ω,k) plane. For, if $k_n^2>(\omega_R^2-\omega_I^2)/c_t^2$, the nonradiative region, $\alpha^2(k_n,\omega)$ is in the third quadrant. This means that $\alpha(k_n,\omega)$ will be in the second quadrant, with a negative real part and a positive imaginary part. The positive imaginary part of $\alpha(k_n,\omega)$ means that the nth term in Eq. (17) decreases exponentially with increasing x_3, as is required of a surface wave. When $k_n^2<(\omega_R^2-\omega_I^2)/c_t^2$, the radiative region, $\alpha^2(k_n,\omega)$ is in the fourth quadrant. Therefore $\alpha(k_n,\omega)$ is also in the fourth quadrant, with a positive real part and a negative imaginary part. The positive real part of $\alpha(k_n,\omega)$ corresponds to a wave that is radiating from the surface into the elastic medium, as we wish for a radiative or leaky surface wave. The negative imaginary part of $\alpha(k_n,\omega)$ in this case corresponds to a wave whose amplitude increases exponentially with increasing x_3. This exponential increase of the amplitude of a leaky surface acoustic wave with increasing distance from the surface is physically correct. It has been discussed in detail by Lim and Farnell [15], by Ingebrigtsen and Tonning [16], and by Glass and Maradudin [17], and the reader is referred to these papers for an explanation of this counterintuitive result.

4. Numerical solution of Eq. (16)

To obtain the dispersion curves for the surface acoustic waves, we followed closely the procedure described in Ref. 7 for solving Eq. (16) numerically. This method begins by approximating the infinite-dimensional matrix entering it by a finite one. To this end, one restricts the indices m and n in Eq. (16) to the values $m,n=-\mathcal{M},-\mathcal{M}+1,\ldots,\mathcal{M}-1,\mathcal{M}$, where $\mathcal{M}$ is a positive integer. We thus seek the values of ω for a given value of k at which the determinant of the resulting $(2\mathcal{M}+1)$-dimensional square matrix vanishes. Instead of using $D(k,\omega)$ directly in a search for its zeros, it was argued in Ref. 7 that it is more convenient in numerical calculations to work with the function

$$\Lambda(k,\omega)=\min\left\{\left|\lambda_m(k,\omega)\right|\right\}_{m=-\mathcal{M}}^{\mathcal{M}}, \tag{20}$$

as it is a smoother function of its arguments and of smaller range than $D(k,\omega)$. In Eq. (20), λ_m denotes an eigenvalue of the $(2\mathcal{M}+1)\times(2\mathcal{M}+1)$ matrix whose determinant is $D(k,\omega)$. Since $D(k,\omega)=\Pi_{m=-\mathcal{M}}^{\mathcal{M}}\lambda_m(k,\omega)$, it follows that the condition $D(k,\omega)=0$ is equivalent to $\Lambda(k,\omega)=0$ which, therefore, represents an alternative definition of the dispersion relation for surface waves on which the numerical calculations presented in this work are based.

To obtain the dispersion curve for the surface waves a mesh of $\mathcal{N}+1$ equally spaced points $k_\ell=\ell\Delta k$, with $\ell=0,1,2\ldots,\mathcal{N}$ and $\Delta k=(\pi/a)/\mathcal{N}$ is created in the interval $(0,\pi/a)$ of the k axis, where $\mathcal{N}$ is typically 100. For each value k_ℓ an independent numerical minimization of the function $\Lambda(k_\ell,\omega)$ is performed with respect to the complex frequency $\omega(k_\ell)=\omega_R(k_\ell)-i\omega_I(k_\ell)$. The minimization is performed using the Nelder–Mead optimization algorithm [18–20] by considering Λ to be a function of two real variables, $\omega_R(k_\ell)$ and $\omega_I(k_\ell)$ $(\omega_R>0,\omega_I>0)$, with k_ℓ treated as a known parameter.

To obtain the first (fundamental) branch of the dispersion curve, corresponding to a true surface wave, the minimization was started at $k_0=0$ with the initial values $\omega_R(k_0)=\omega_I(k_0)=0$; as ℓ was increased, the initial values for ω_R and ω_I when performing the minimization at k_ℓ were $\omega_R(k_{\ell-1})$ and $\omega_I(k_{\ell-1})$, respectively. In this way the first branch of the dispersion curve was determined. It is worth noting that these calculations produced a vanishing imaginary part for the frequency, as is expected for a branch that lies in the nonradiative region of the (k,ω) plane. To be certain that the value of $\omega(k_\ell)$ obtained this way is on the dispersion curve for surface acoustic waves we recorded both the eigenvalue of the matrix $\mathbf{M}(k_\ell,\omega)$ with the smallest modulus, and its reciprocal condition number. When the calculations were performed in double precision, these quantities were found to be at least as small as 10^{-15} and 10^{-16}, respectively.

In obtaining the numerical results for the higher frequency branches presented in the next section, the initial values $\omega_R a/c_t\pi=n-1$ and $\omega_I a/c_t\pi=0$ were used successfully for the first k point of the nth branch of the dispersion curve situated on the left (odd branches) or right (even branches) boundary of the first Brillouin zone. For the remaining k_ℓ values $(\ell>0)$ on a higher frequency branch we again used $\omega_R(k_{\ell-1})$ and $\omega_I(k_{\ell-1})$ as the initial values for the complex frequency in the minimization routine. In this manner the second and third branches of the dispersion curve were determined.

5. Results

We illustrate the preceding results by presenting results for the dependence of the reflectivity and several other diffraction efficiencies on the angle of incidence θ_0, when the sinusoidal grating defined by the surface profile function

$$\zeta(x_1)=\zeta_0\cos\left(\frac{2\pi x_1}{a}\right) \tag{21}$$

is illuminated by a bulk wave of shear horizontal polarization of frequency ω. For this profile function, the function $\mathcal{I}_p(\gamma)$ defined by Eq. (8) is given by

$$\mathcal{I}_p(\gamma)=(i)^p J_p(\gamma\zeta_0), \tag{22}$$

where $J_p(z)$ is a Bessel function of the first kind and order p.

To help in interpreting the results for the diffraction efficiencies we note that the values of θ_0 at which the Rayleigh anomalies are expected to occur are obtained from the equation

$$\sin\theta_0^{(m)}=\pm1+m\frac{\lambda}{a}, \tag{23}$$

where m is an integer, λ is the wavelength of the incident wave, and a is the period of the grating.

The values of θ_0 at which Wood anomalies are expected to occur are obtained from the equation

$$\frac{\omega}{c}\sin\theta_0=k_s(\omega)+n\frac{2\pi}{a}, \tag{24}$$

where $k_s(\omega)$ is the wavenumber of the shear horizontal surface acoustic wave the real part of whose frequency is that of the incident acoustic wave. It is convenient to rewrite Eq. (24) as

$$\sin\theta_0=\frac{\lambda}{a}\left[\frac{1}{2}\frac{k_s(\omega)a}{\pi}+n\right]. \tag{25}$$

The value of $k_s(\omega)$ is confined to the interval $0\le k_s(\omega)\le\pi/a$.

The grating we consider in our examples is defined by Eq. (21) with $\zeta_0/a=0.40$. The dispersion curve for the surface acoustic wave supported by this grating, plotted in the reduced zone scheme, is depicted in the left-hand panel of Fig. 2, where $\omega_R(k)$ is plotted as a function of k. It con-

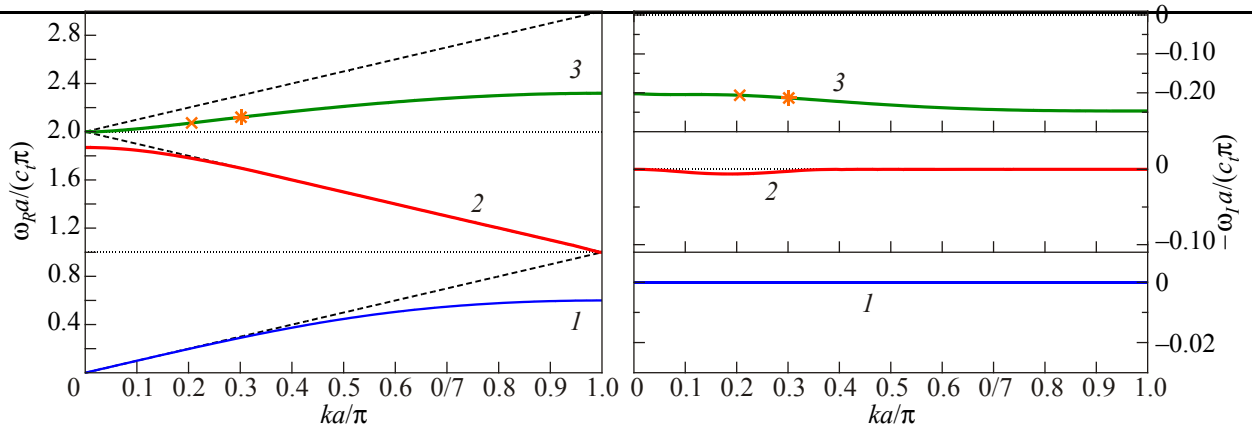

Fig. 2. (Color online) The dispersion curves for the shear horizontal surface acoustic waves supported by a sinusoidal grating on an isotropic elastic medium in contact with vacuum defined by $\zeta_0 / a = 0.40$. Both the real, $\omega_R(k)$, and imaginary, $\omega_I(k)$, parts of the frequencies of the waves are presented in the reduced zone scheme. The first branch of the dispersion curve (line *1*) lies in the nonradiative region of the (k,ω) plane, and corresponds to a true surface wave, the imaginary part of whose frequency vanishes identically. The second and third branches of the dispersion curve (lines *2* and *3*, respectively) are both situated in the radiative region ($|k| < \omega/c_t$). They correspond to leaky surface waves, whose frequencies have negative imaginary parts. The dashed lines denote the dispersion curve $\omega = c_t k$ in the absence of the surface corrugations in the reduced zone scheme. Also indicated are the wavelengths $\lambda / a = 0.9653$ [$\omega a / c_t\pi = 2.0718$; symbol ×] and $\lambda / a = 0.9421$ [$\omega a / c_t\pi = 2.1228$; symbol ∗] of the incident acoustic wave that will be assumed in the calculations of the diffraction efficiencies plotted in Figs. 3 and 4, respectively.

sists an infinite number of branches, of which we present only the three with the lowest frequencies. The right-hand panel presents plots of $\omega_I(k)$ as a function of k for each branch of the dispersion curve plotted in the left-hand panel. The magnitude of $\omega_I(k)$ gives an indication of the width of the Wood anomaly. We also present in the left-hand panel the dispersion curve of the "surface" wave in the absence of the periodic corrugations of the surface, $\omega = c_t k$, when it is folded back into the first Brillouin zone.

In Fig. 3 we present the dependencies of the first several diffraction efficiencies of this grating on the angle of incidence θ_0. The wavelength of the incident shear horizontal acoustic waves assumed in obtaining these results was $\lambda / a = 0.9653$ [$\omega a / c_t\pi = 2.0718$]. This corresponds to a point on the third branch of the dispersion curve plotted in Fig. 2 defined by $k_s(\omega)a/\pi = 0.2041$ [symbol × in Fig. 2]. For these values of the grating and experimental parameters Eq. (23) predicts that Rayleigh anomalies should occur at $\theta_0 = \pm 1.99^\circ$ and $\pm 68.54^\circ$, while Eq. (25) predicts that Wood anomalies should occur at $\theta_0 = \pm 5.65^\circ$ and $\pm 60.09^\circ$. The predicted angular positions of the Rayleigh and Wood anomalies are indicated by dash-dotted and dashed vertical lines, respectively, in this and the next figure. In the results presented in Fig. 3 the Rayleigh and Wood anomalies appear at the angles of incidence predicted for them by Eqs. (23) and (25), respectively. In the case of $e_0(\theta_0)$ (the reflectivity) the Rayleigh anomalies at $\theta_0 = \pm 1.99^\circ$ and $\pm 68.54^\circ$ are vertical slopes, while the Wood anomalies at $\theta_0 = \pm 5.65^\circ$ and $\pm 60.09^\circ$ are peaks. In the results presented for $e_{-1}(\theta_0)$ the Rayleigh anomalies at $\theta_0 = 1.99^\circ$ and 68.54° are sharp peaks, while the one at $\theta_0 = -1.99^\circ$ is a vertical slope. The Wood anomalies at $\theta_0 = 5.65^\circ$ and 60.09° are now dips. In the result for $e_1(\theta_0)$ the Rayleigh anomaly at $\theta_0 = -1.99^\circ$ becomes a sharp peak, while the one at $\theta_0 = 1.99^\circ$ is now a vertical slope. There are no Wood anomalies in the angular dependence of this diffraction

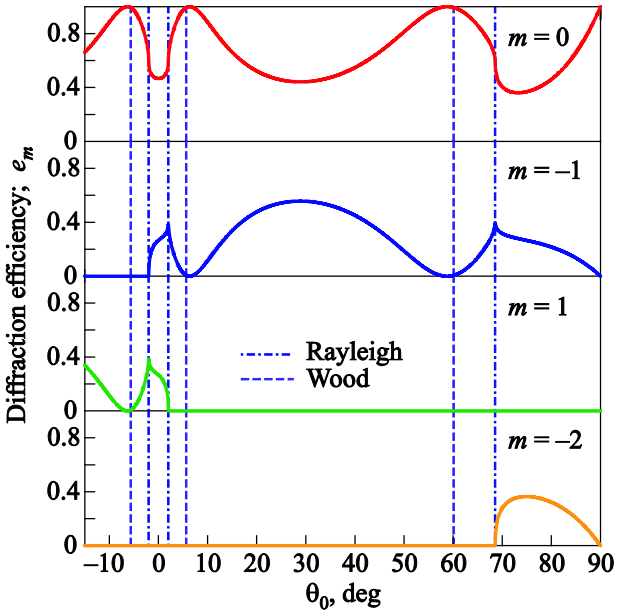

Fig. 3. (Color online) The diffraction efficiencies $e_m(\theta_0)$, Eq. (11), as functions of the angle of incidence for a sinusoidal grating defined by $\zeta_0 / a = 0.40$. The angular positions of the Rayleigh and Wood anomalies, determined from Eqs. (23) and (25), respectively, are indicated by vertical dash-dotted and dashed lines, respectively. Only diffracted orders m for which $e_m(\theta_0) \neq 0$ in the range of θ_0 considered are presented. The wavelength of the incident acoustic wave assumed in obtaining these results was $\lambda / a = 0.9653$ [$\omega a / c_t\pi = 2.0718$; symbol × in Fig. 2].

efficiency. In the result for $e_{-2}(\theta_0)$ the Rayleigh anomaly at $\theta_0 = 68.54^\circ$ is represented by the appearance of a new diffracted order as θ_0 is increased, while no Wood anomalies are present.

In the numerical calculations that produced Figs. 2 and 3, a value of $\mathcal{M} = 10$ was used, because increasing it beyond this value did not produce any detectable changes in the results obtained for the grating parameters assumed. In addition, the energy conservation condition Eq. (12) was checked explicitly and, for all angles of incidence considered the left-hand side of this equation was found to depart from unity by an amount no larger than 10^{-12} in magnitude when the calculations were carried out in double precision.

As a second example to illustrate our results, we again consider the sinusoidal grating defined by Eq. (21) with $\zeta_0 / a = 0.40$. The dispersion curve of the surface acoustic waves of shear horizontal polarization supported by this grating is depicted in Fig. 2. The surface is now illuminated by a shear horizontal polarized volume acoustic wave whose wavelength is $\lambda / a = 0.9421$ $[\omega a / c_t \pi = 2.1228]$. This corresponds to the point on the third branch of the dispersion curve defined by $k_s(\omega)a / \pi = 0.3061$ [symbol $*$ in Fig. 2]. Under these conditions Eq. (23) predicts Rayleigh anomalies to occur at $\theta_0 = \pm 3.31^\circ$ and $\pm 62.17^\circ$, while Eq. (25) predicts Wood anomalies to occur at $\theta_0 = \pm 8.29^\circ$ and $\pm 52.93^\circ$. In the results for the dependencies of several of the lowest order diffraction efficiencies on the angle of incidence θ_0 presented in Fig. 4, the Rayleigh and Wood anomalies are seen to occur at these angles. When the results presented in Fig. 4 are compared with those presented in Fig. 3, it is seen that although the angular positions of the anomalies have changed with the change of the wavelength of the incident waves, their natures have not: vertical slopes remain vertical slopes, peaks remain peaks, and dips remain dips.

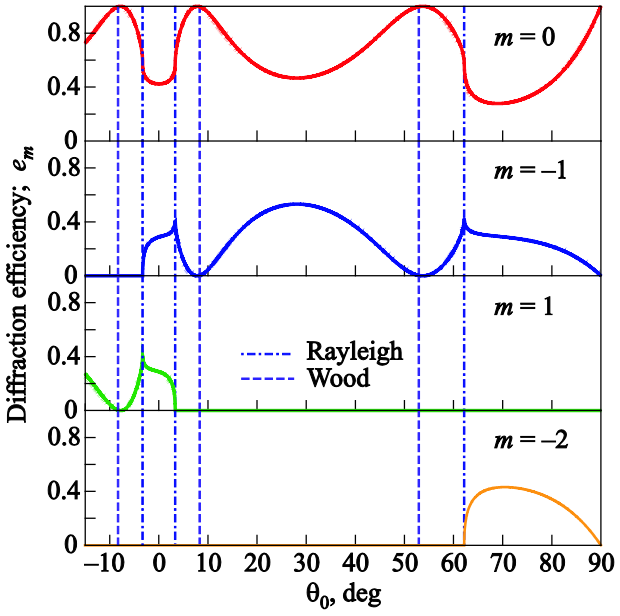

Fig. 4. (Color online) The same as Fig. 3, but for a wavelength of the incident acoustic wave $\lambda / a = 0.9421$ $[\omega a / c_t \pi = 2.1228$; symbol $*$ in Fig. 2].

The results presented in Fig. 4 were calculated using double precision with $\mathcal{M} = 10$. The satisfaction of unitarity by the results was as good as for those depicted in Fig. 3.

6. Conclusions

We have shown that when the periodically corrugated surface of an isotropic elastic medium is illuminated by a shear horizontal volume acoustic wave, the dependencies of the diffraction efficiencies on the angle of incidence display features that can be identified as Rayleigh and Wood anomalies. Unlike the surface plasmon polaritons that play the central role in the formation of Wood anomalies, which exist even in the case of a planar metal surface, the shear horizontal surface acoustic waves responsible for the Wood anomalies studied in this work cannot exist on a planar surface of an isotropic elastic medium. Thus, the periodic corrugations of the surface play different roles in the formation of these anomalies. In the case of a weakly corrugated metal surface, the dispersion curve for surface plasmon polaritons is well represented by the dispersion curve of surface plasmon polaritons on a planar surface, except in the vicinities of the boundaries of the Brillouin zones introduced by the periodicity of its corrugations. The principle role of the corrugations in the formation of Wood anomalies is the formation of these Brillouin zones. If the dielectric function of the metal is denoted by $\varepsilon(\omega)$, the wavenumber of the surface plasmon polariton of frequency ω on a planar surface is $k_{spp}(\omega) = (\omega / c)[\varepsilon(\omega) / (\varepsilon(\omega) + 1)]^{1/2}$. Thus, a good approximation to the angles of incidence at which Wood anomalies will appear is obtained from

$$\frac{\omega}{c}\sin\theta_0 = \frac{\omega}{c}\left[\frac{\varepsilon(\omega)}{\varepsilon(\omega)+1}\right]^{1/2} + \frac{2\pi n}{a}. \qquad (26)$$

The function $k_{spp}(\omega)$ can deviate significantly from the wavenumber of the vacuum light line, $k(\omega) = \omega / c$. This is an important feature of this $k_{spp}(\omega)$, because if it were to coincide with $k(\omega)$, the angular positions of the Wood anomalies would coincide with those of the Rayleigh anomalies, and would be indistinguishable from them.

This is just the situation encountered in the problem studied here. The dispersion relation for shear horizontal surface acoustic waves on a planar surface of an isotropic solid coincides with the acoustic sound line $k(\omega) = \omega / c_t$. Therefore any attempt to use it in estimating the angles of incidence at which Wood anomalies occur would yield only the angles at which Rayleigh anomalies occur. The role of the corrugations is crucial here. They not only produce a Brillouin zone structure but, more important, produce a dispersion curve whose branches depart sufficiently far from the acoustical sound line that the Wood anomalies

that are created in the angular dependence of the diffraction efficiencies occur at angles of incidence sufficiently far from those at which the Rayleigh anomalies occur, that they are clearly visible.

In the course of this work we have had to calculate the complex dispersion curves of the shear horizontal surface acoustic waves supported by the periodically corrugated surface in the nonradiative region of the frequency-wavenumber plane. To our knowledge such calculations have not been carried out until now. The results of such calculations could be useful in studies of the attenuation of shear horizontal surface acoustic waves on a periodically corrugated surface, as proved to be the case in the study of the attenuation of sagittal, Rayleigh, surface acoustic waves on such surfaces [17].

Finally, we see from the figures presented here that the Rayleigh and Wood anomalies are strong enough to be observable experimentally. It is our hope that such experiments will be undertaken.

Acknowledgments

We dedicate this paper to the memory of Professor K.B. Tolpygo, on the occasion of his 100-year anniversary. He was a fine scholar and a fine person, whom it was a pleasure to know. The research of I.S. was supported in part by the Research Council of Norway Contract No. 216699.

1. B.A. Auld, J.J. Gagnepain, and M. Tan, *Electron. Lett.* **12**, 650 (1976).
2. Yu.V. Gulyaev and V.P. Plesskii, *Sov. Phys. Tech. Phys*. **23**, 266 (1978).
3. N.E. Glass and A.A. Maradudin, *Electron. Lett.* **17**, 773 (1981).
4. D.L. Mills and A.A. Maradudin, *Phys. Rev. B* **39**, 1569 (1989).
5. J.B. Pendry, L. Martn-Moreno, and F.J. Garca-Vidal, *Science* **305**, 847 (2004).
6. A.R. Baghai-Wadji and A.A. Maradudin, *Appl. Phys. Lett.* **59**, 1841 (1991).
7. A.A. Maradudin, I. Simonsen, J. Polanco, and R.M. Fitzgerald, *J. Optics* **18**, 024004 (2016).
8. R.W. Wood, *Philos. Mag.* **4**, 396 (1902).
9. R.W. Wood, *Proc. Phys. Soc. (London)* **18**, 269 (1902).
10. Lord Rayleigh, *Proc. Roy. Soc. (London) A* **79**, 399 (1907).
11. Lord Rayleigh, *Philos. Mag*. **14**, 60 (1907).
12. U. Fano, *J. Opt. Soc. Am*. **3**, 213 (1941).
13. S.A. Maier, *Plasmonics: Fundamentals and Applications*, Springer US, New York (2007).
14. Lord Rayleigh, *The Theory of Sound*, Vol. II, 2nd ed., Macmillan, London (1897), pp. 89, 297.
15. T.C. Lim and G.W. Farnell, *J. Acoust. Soc. Am*. **45**, 845 (1969).
16. K.A. Ingebrigtsen and A. Tonning, *Phys. Rev.* **184**, 942 (1969).
17. N.E. Glass and A.A. Maradudin, *J. Appl. Phys.* **54**, 796 (1983).
18. J.A. Nelder and R. Mead, *Computer J*. **7**, 308 (1965).
19. R. O'Neill, *Appl. Stat*. **20**, 338 (1971).
20. J.C. Lagarias, J.A. Reeds, M.H. Wright, and P.E. Wright, *SIAM J. Optim*. **9**, 112 (1998).